PIER C

(Received 25 August 2025, Accepted 22 October 2025, Scheduled 6 November 2025)

Design a Type of Analog Beamforming MIMO System Based on a Rotman Lens with an Ultra-Wideband (UWB) for 5G mmWave Applications

Noureddine Boughaba[1,*], Ouarda Barkat[2], and Khaled Issa[3]

[1] *Electromagnetism and Telecommunications Laboratory, Department of Electronics University Frères Mentouri Constantine 1, Algeria*
[2] *Department of Electronics, University Frères Mentouri Constantine 1, Algeria*
[3] *Laboratory of Electronics and Microelectronics, Department of Physics Faculty of Sciences of Monastir, University of Monastir, Tunisia*

ABSTRACT: High frequency communication systems are critical for 5G networks, particularly in the millimeter-wave bands, where ultra-wideband (5G-UWB) performance is essential for high data rates and low latency. In this work, we propose, for the first time to the best of our knowledge, an ultra-wideband 5G MIMO beamforming module covering both the 28 and 60 GHz bands. The proposed design is based on a low-cost, low-profile Rotman Lens (RL) implemented on an FR4 substrate with a thickness of 1.6 mm and a dielectric constant of 4.3. The RL features five beam ports and seven array ports, with additional dummy ports introduced to minimize reflections and enhance adjacent beam port isolation across the full 5G-UWB range. Simulation results demonstrate excellent performance, with isolation and mutual coupling maintained below –25 dB between input beam ports and below –15 dB between array ports across the entire bandwidth. The VSWR remains below 2 for all ports. Although this work presents a single RL-based beamformer, it is envisioned as a building block within a larger hybrid MIMO architecture, where multiple lenses can be interconnected to support parallel data streams and spatial multiplexing. This modular approach enables flexible scaling to full MIMO operation while maintaining low cost and compactness. The proposed design is a strong candidate for 5G and mmWave applications, including hybrid beamforming systems, MIMO architectures, radar, and satellite communications. Comparative analysis with recent literature demonstrates its superior bandwidth and isolation performance.

1. INTRODUCTION

Due to recent advancements in 5G technologies, millimeter-wave (mmWave) technology has enabled the emergence of Internet of Things (IoT) devices, providing extensive connectivity, minimal latency, and rapid data transmission. These capabilities are crucial for advanced applications such as smart cities, self-driving cars, and industrial automation [1, 2]. MmWave approach has attracted significant interest due to its ability to address the growing demands of 5G communication systems, providing higher reliability, and support for large-scale device connectivity [3, 4]. The mmWave range also enables the development of smart and cost-effective wireless technologies and devices, offering reduced power consumption and system complexity, which are essential for supporting modern multimedia applications. These enhanced capabilities are achieved through the ultra-wide bandwidth with the shift to higher frequencies. This shift is largely motivated by spectrum congestion below 6 GHz, where numerous wireless standards coexist [5, 6]. Additionally, frequencies such as sub-6 GHz, 28 GHz, and 38 GHz are increasingly explored for 5G networks [7, 8]. The 3rd Generation Partnership Project (3GPP) has designated multiple frequency bands within mmWave range, particularly the globally harmonized 28 GHz bands (n257, n258, and n261), which simplify device manufacturing and attract considerable interest from both academia and industry [9]. Moreover, the 60 GHz frequency range, known as V-band, has been widely recommended by the Federal Communications Commission (FCC) for scientific, medical, and high-rate communication purposes. Due to its favorable propagation characteristics and the availability of 7 GHz of unlicensed spectrum [10], this band is widely explored. This makes it ideal for establishing secure, short- to mid-range indoor and outdoor links with frequency reuse capabilities. In this context, standards such as IEEE 802.11ad and IEEE 802.15.3c have emerged to support high-data-rate wireless communication at 60 GHz, paving the way for multi-Gbps channels and efficient RF access technologies [11]. However, harnessing mmWave frequencies for future wireless networks presents unique technical challenges. The higher frequencies in this band suffer from increased free-space path loss and reduced ability to penetrate physical barriers such as walls and buildings [12]. However, the concentration of the wave in a specific, dynamic direction known as beamforming technics may solve this issue. Beamforming is recognized as one of the key enablers of 5G due to its critical role in ensuring reliable, high-capacity

* Corresponding author: Noureddine Boughaba (boughabanoureddine13@gmail.com).

communication [7]. Among various beamforming techniques, analog beamforming stands out for its simplicity and low cost compared to digital approaches [13]. It enables the concentration of signal energy toward desired directions while suppressing interference from others, effectively mitigating path loss and signal attenuation. This directional control enhances coverage and system performance, particularly in challenging environments such as dense urban or remote rural areas. The importance of beamforming becomes even more pronounced at millimeter-wave frequencies, where the trade-off between shorter range and higher data rates demands precise and efficient signal steering [14].

Several analog RF beamforming networks (BFNs) have been proposed and are usually separated into two primary groups: Beamformers based on lenses, such the Rotman lens [15] and circuit-based beamformers [16]. One of the most widely adopted circuit-based architectures is Butler Matrix (BM), valued for its simple structure, low cost, and ease of fabrication. It is commonly employed to feed phased antenna arrays, especially in mmWave multibeam applications [17, 18]. Phase shifters, crossovers, and hybrid couplers define a standard Butler matrix. However, its narrow operational bandwidth mainly due to the phase shifters limits its effectiveness in wideband scenarios. Nonetheless, the limited bandwidth of operation due to the phase shifters limits its effectiveness in wideband scenarios.

On the other hand, the Rotman lens (RL) stands out as a promising massive passive microwave lens-based BFN, offering benefits like structural and operational simplicity, low cost, easy implementation, and a broad scanning angle [19]. Operating as a passive phase-shifting network inspired by the principles of geometrical optics [20], it stands out due to its framework consisting of switchable input and output ports that connect to an antenna array, allowing the formation of discrete beams in different directions [21]. As a real time delay (RTD) beamforming network, the Rotman lens operates independently of frequency, which provides it with wide bandwidth and excellent adaptability to multibeam systems [21, 22]. Recent studies on the Rotman lens have focused on improving electrical characteristics and making modifications for Custom applications. Main advancements include expanding the scanning angle [3, 4, 23], compacting or reducing lens dimensions [24, 25], reducing phase error [26], and wide bandwidth [27]. A variety of materials and fabrication technologies, such as printed circuit boards (PCBs), substrate integrated waveguides (SIWs), ridge gap waveguides (RGWs), substrate-integrated coaxial lines (SICLs), and low-temperature co-fired ceramic (LTCC) technology, can be used to implement the Rotman lens due to its lightweight, cost-effective, and compact structure [3, 11, 12, 28, 29].

For 5G applications, high-frequency bands such as 24 GHz (n258), 28 GHz (n257 and n261), 37 GHz (n260), 39 GHz (n260), and upcoming bands like 47 and 60 GHz have recently been explored. These mmWave bands offer significantly large bandwidths (over 500 MHz) [30]. In this study, the proposed Rotman lens is designed for covering a dual-band frequency of 28 and 60 GHz, making it one of the potential candidates for fifth-generation wireless networks. This lens covers the mmWave frequency bands defined by 3GPP for 5G systems, including bands n257, n258, n259, n260, n261, and n262 [3, 5, 31]. The Rotman lens is designed following Hansen's procedure to optimize its parameters, maximizing gain while minimizing phase error. With a broad bandwidth covering from 23 GHz to 65 GHz, the Rotman lens based on an FR-4 substrate is evaluated using CST Microwave Studio (CST MWS), which analyzes input ports, return loss, and coupling between beam and antenna ports. The analog beamforming network with minimal loss and low cost has been designed using printed circuit board technology. This is the structure of the article. The Rotman lens's geometric design is shown in Section 2. It is based on Hansen's modified version of Rotman and Turner equations. The Rotman lens's final prototype is also shown in this part, along with a thorough analysis of surface currents and the characterization of S-parameters such as coupling, transmission, and reflection coefficients. Finally, the conclusion is presented in the third section.

2. ROTMAN LENS CONFIGURATION DESIGN

RL, introduced by Rotman and Turner in 1963, is a beamforming network widely used to feed linear antenna arrays [32]. Numerous methods have been put forth to enhance Rotman lens's performance, either through applying advanced optimization techniques [33–35] or by altering its geometry, as demonstrated by the updates from Katagi et al. [36] and Hansen [33]. It was thought that the inner receiving outlines and the beam were circular in Rotman's original design [32]. In order to minimize the error in path length, Hansen [33] suggested an elliptical beam contour. Owing to its broadband and wide-angle beamforming capabilities, Rotman lens is especially relevant for 5G multibeam antenna systems.

In this study, the design equations and processes suggested in [33] are used to define geometric specifications of the Rotman lens. The detailed procedure for establishing the initial geometry according to this approach is demonstrated in recent studies [3, 37, 38]. Its design concepts are based on geometrical optics (GO) theory, which enables the precise determination of the placement of beam ports on the focal arc and antenna ports on the inner contour [3]. The Rotman lens, inspired by optical concepts, functions as a multi-port microwave circuit. The Rotman lens geometry is characterized by three focal points, as adjusted by Hansen and illustrated in Figure 1. They are positioned on a circular or elliptical focal arc, also known as beam contour, which ensures that no phase errors occur at the beam ports. The central focal point F_0 lies on the main axis (on-axis focal point) and corresponds to the on-axis focal length f_1, while F_1 and F_2 are symmetrically placed at $\pm\alpha$ on the focal arc (off-axis focal points) and correspond to the off-axis focal length f_2. The focal angles α are defined as the angles subtended by these off-axis foci (F_1 and F_2) at the center of the element ports curve in the case of a symmetrical lens geometry, with f_1 also representing the lens width at the center.

The position of the array element (N), the placement of array ports along the array axis of a typical radiating element (y_3), the electrical length connecting array ports and elements, and the

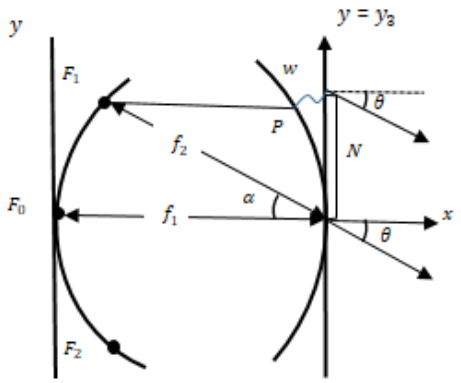

FIGURE 1. Rotman lens structure modified by Hansen.

beamsteering angle (θ) correspond to the off-center focal point. Hansen [33] introduced four essential parameters $(\alpha, \beta, f_1, \gamma)$ which define the lens configuration and allow for the normalization of all dimensions based on f_1.

Moreover, known as the focal ratio and indicated by β, this focal parameter is calculated by dividing the upper focal length f_2 by the lower focal length f_1 as:

$$\beta = \frac{f_2}{f_1} \tag{1}$$

Defined as the angle ratio between the excited off-axis foci and the array, the expansion factor (γ) is given in terms of array beam angle (θ) and lens array angle (α) by:

$$\gamma = \frac{\sin(\theta)}{\sin(\alpha)} \tag{2}$$

The array elements at $y = y_3$ are connected to an additional delay line by the normalized cable electrical length (w) in order to achieve phase shift. The quadratic equations are as follows [3, 33, 34, 39]:

$$\alpha \left(\frac{W}{f_1}\right)^2 + b\left(\frac{W}{f_1}\right) + c = 0 \tag{3}$$

The normalized relative transmission line length w is determined by the maximum scanning angle (θ) and focal angle (α) parameters. The quadratic equation's solutions, a, b, and c, are defined as follows:

$$\alpha = 1 - \left(\frac{1-\beta}{1-\beta C}\right)^2 - \frac{\zeta^2}{\beta^2} \tag{4}$$

$$b = 2 - \frac{2\zeta^2}{\beta} + \frac{2(1-\beta)}{1-\beta C} - \frac{\zeta^2 S^2(1-\beta)}{(1-\beta C)^2} \tag{5}$$

$$c = -\zeta^2 + \frac{\zeta^2 S^2}{1-\beta C} - \frac{\zeta^2 S^4}{4(1-\beta C)} \tag{6}$$

$$S = \sin\alpha, \qquad C = \cos\alpha$$

ζ is an indirect parameter used to adjust the portion of the lens's phase and amplitude error curve, expressed by the equation:

$$\zeta = \frac{y_3\,\gamma}{f_1} \tag{7}$$

The value of parameter ζ varies according to the position y_3 of each point on the array relative to the axis toward f_1, which also influences the phase. The number of beam ports is selected based on the necessary beam directions. In this configuration, the Rotman lens enables five beam directions, and the number of antennas is seven. The configuration parameters influence the structure of the Rotman lens in the millimeter-wave band, as well as its phase error and gain performance. The phase center locations of the ports are determined using carefully defined geometric parameters and certain optimization factors. In this section, the effects of the focal angle α, focal ratio β, and ray-to-beam angle ratio (γ) are studied. These considerations are then summarized in a simplified design methodology for developing an optimal beamforming network (BFN) based on a Rotman lens. Further details can be found in [33–35]. Accordingly, Figures 2 and 3 present the study of the influence of the α and β parameters on the geometry of the Rotman lens. The value of α is used to approximate the equalization of contour curvature and to define the position of the ports. To obtain nearly equivalent lens shapes and port positions, the effect of β on the lens's shape is observed to be comparable to that of α. When the value of α is reduced, the beam contour shifts toward the center, in contrast to the receiving contour. As illustrated and mentioned in previous studies [33, 37], the receiving contour becomes flatter as α decreases. This can influence the fabrication process of the lens, as a growing α value increases the structure's dimensions. Although α and β significantly affect the lens's apparent shape, it is essential to select them in combination with other parameters to ensure acceptable amplitude levels and minimize phase deviations. For a given maximum scan angle, it is possible to adjust the ratio between the focal angle and array beam angle to meet the design requirements. In this case, the expansion factor γ is considered. In this context, a value of γ greater than one is chosen to enable large beam scanning angles, specifically 30°, as illustrated in Figure 4. It is observed that as the value of γ increases, the beam contour expands while the output contour contracts, and the distance between the phase center of the output ports decreases.

To design and model the RL structure, we need a Matlab code to generate the equations presented in [3, 32, 34, 37]. According to this study, the lens cavity and transmission lines should use the same permittivity substrate material as [37]. Table 1 details the optimized parameters and their corresponding values, reflecting the specific design characteristics of the proposed Rotman lens. By solving the design equations, a MATLAB code was used to produce the coordinates of beam ports and output ports, as shown in Figure 5. A crucial component of the design is taper transition, which modifies flare angles of the ports to ensure seamless energy transfer from the input ports via the aperture parallel plate to the receiver ports and radiating elements. To minimize phase error and facilitate the use of microstrip-line feed excitation through the antenna, an additional transmission line of the same length is added at the start of each taper [39].

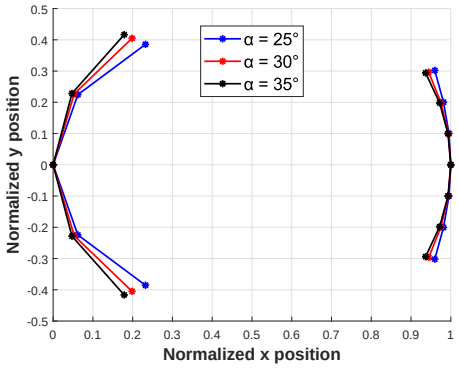

FIGURE 2. Effect of the α parameter on the shape of the RL.

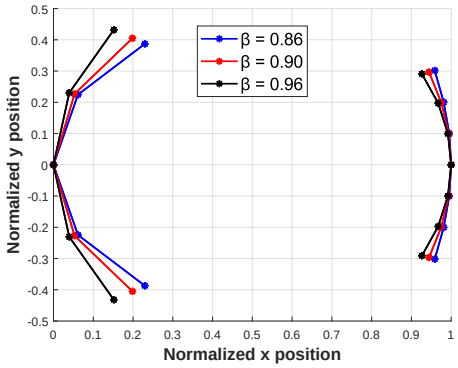

FIGURE 3. Effect of the β parameter on the shape of the RL.

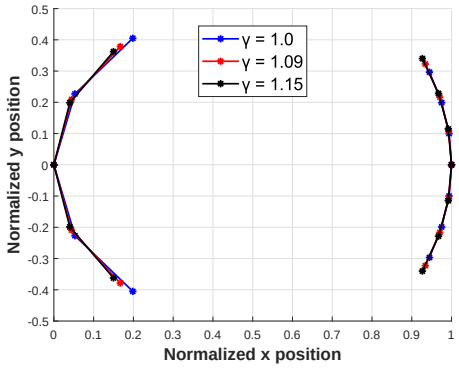

FIGURE 4. Effect of the γ on the RL geometry.

TABLE 1. Design parameters of the Rotman lens.

Design parameters	Values	Design parameters	Values
Design frequency (f_0)	28 GHz	Focal ratio (β)	0.9
Beam ports (N_b)	5	Antenna element spacing (d)	0.5λ
Array ports (N_a)	7	Array steering angle (θ)	30°
Dummy ports (N_d)	8	Focal angle (α)	30°

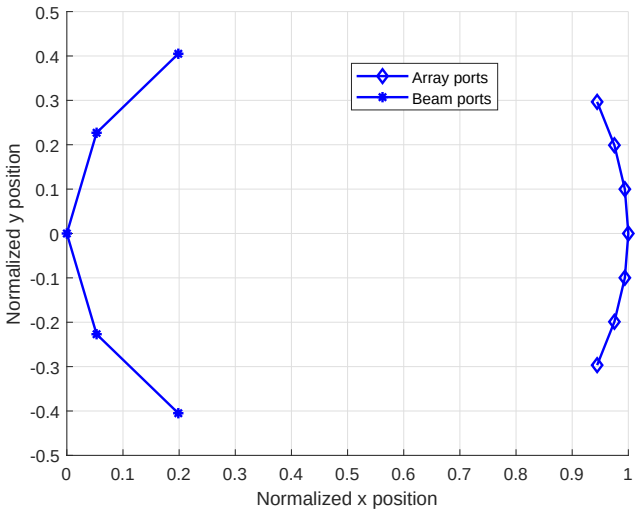

FIGURE 5. Position of beam ports and array ports.

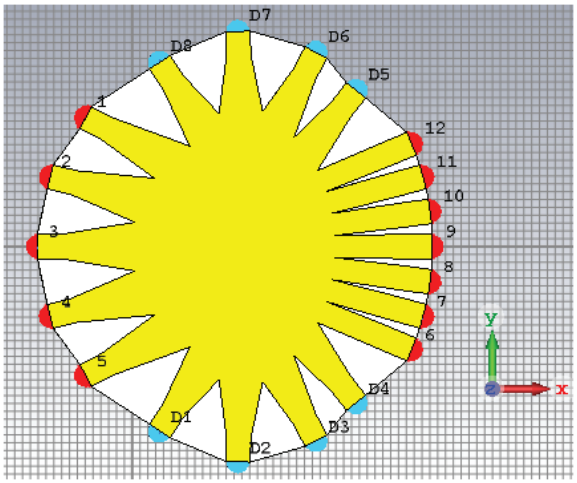

FIGURE 6. Rotman lens structure in CST.

This work employs a model based on an FR-4 substrate, characterized by a dielectric constant of 4.3, a thickness of 1.6 mm, a loss tangent of 0.025, and copper cladding layers of 35 µm on both the top and bottom surfaces. The final Rotman lens structure, illustrated in Figure 6, comprises five beam ports that enable beam scanning from −30° to 30°. It also includes eight array ports and eight dummy ports, labeled D_1 to D_8 and shown in blue in Figure 6. The introduction of dummy ports between the input and output ports of the Rotman lens significantly reduces mutual coupling among the input ports, thereby enhancing overall performance.

3. SIMULATION AND DISCUSSION RESULTS

In this section, we use CST MWS, which is based on the Finite Element Method (FEM), to show our results.

3.1. Reflection Coefficients

The return loss magnitudes as a function of frequency for the five input beam ports (ports 1 to 5) of the proposed Rotman lens are shown in Figure 7. Due to the symmetry of the designed Rotman lens, the reflection coefficients of port 5 (S_{55}) and port 4 (S_{44}) are identical to those of port 2 (S_{22}) and port 1 (S_{11}), respectively. These results demonstrate excellent performance (< -12 dB) over the entire frequency range from

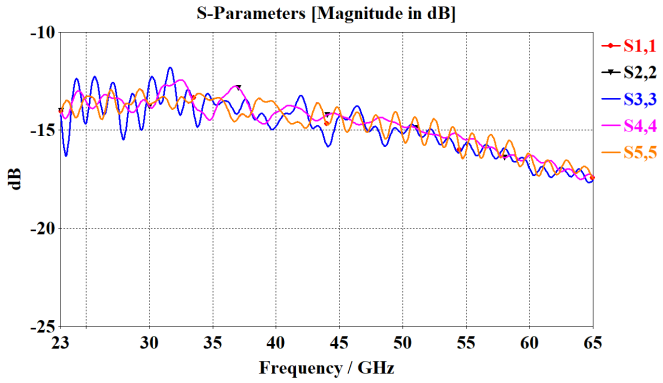

FIGURE 7. Reflection coefficients of beam ports 1 to 5.

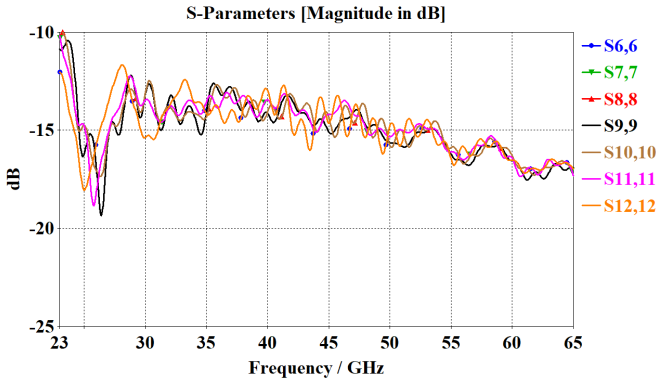

FIGURE 8. Reflection coefficients of array ports 6 to 12.

TABLE 2. Comparisons between this work and other similar works in the references.

Ref	B.Ports	A. Ports	D. Ports	Freq (GHz)	Isol (dB)	BW (%)
[3]	8	8	2	24–40	−28	57.69
[5]	5	8	4	20–45	−20–−45	96.15
[9]	10	10	-	16–32	−15	-
[21]	9	8	6	28–38	-	30.3
[29]	7	5	8	24–30	−20	-
[39]	5	6	8	5.5–6.1	−15–−20	10.34
[40]	7	8	16	23–32	-	21.4
[41]	4	6	6	8–12	−17.2	26.9
[42]	5	6	4	27–29	−20	7.14
[43]	5	10	-	27–29	−20	5.71
[44]	4	6	7	9–15	−15	46.67
[45]	7	7	2	18–22	−15	17.5
This work	5	7	8	23–65	−25	100

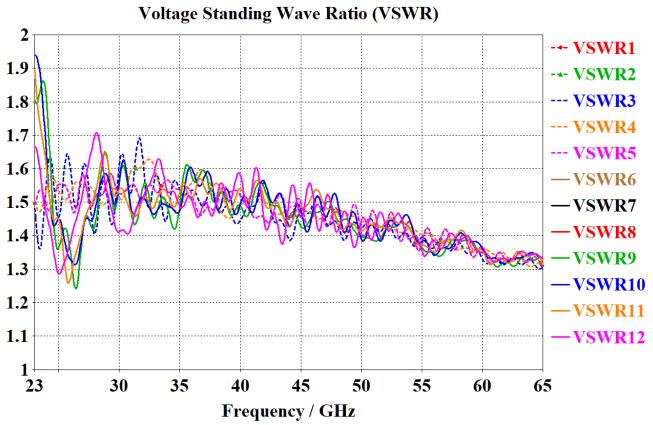

FIGURE 9. VSWR of the beam ports and array ports.

23 GHz to 65 GHz, achieving an average impedance bandwidth about 100% (23–-65 GHz). Furthermore, as shown in Figure 8, the reflection coefficients for the array ports (ports 6 to 12, represented by S_{66} to $S_{12\,12}$) remain below −10 dB across the whole frequency band, confirming suitable impedance matching.

3.2. VSWR (Voltage Standing Wave Ratio)

Figure 9 shows the VSWR for both the beam ports (ports 1-–5, represented by VSWR1–-VSWR5) and array ports (ports 6–-12, represented by VSWR6–-VSWR12). This parameter remains below 2 across all ports throughout the frequency band. Notably, the beam ports maintain a VSWR under 1.7 (dashed line), which is considered satisfactory for most engineering applications.

3.3. Mutual Coupling Between Ports

The coupling between adjacent input ports plays a crucial role in power loss, which is greatly influenced by the distance between the ports and can result in mutual coupling. Figure 10 reports the isolation among all input ports. As shown in Figure 10, the isolation performance is outstanding, with values below −25 dB for both neighboring and remote ports, ensuring minimal electromagnetic (EM) loss between input ports. Coupling effects for the output ports become increasingly significant due to the reduced spacing between transmission lines connecting adjacent network ports compared to those between beam ports. As illustrated in Figure 11, the coupling observed at the output network ports is notably higher than that at the

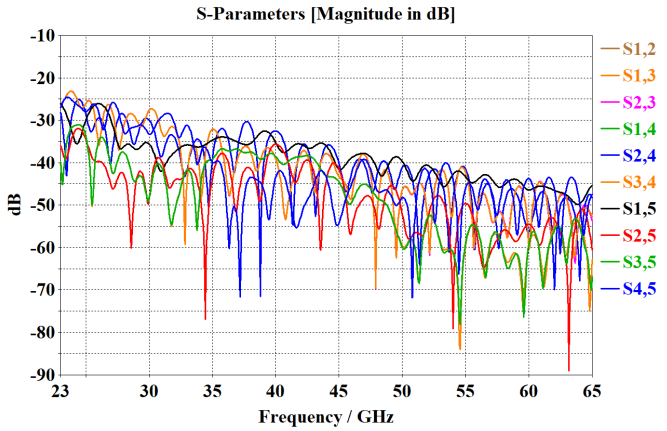

FIGURE 10. Mutual coupling between input ports.

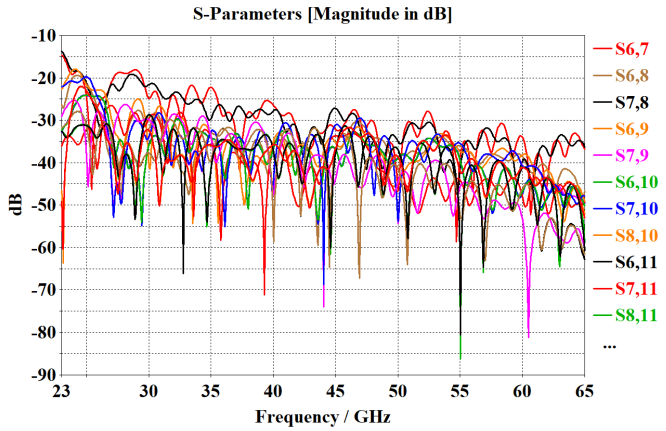

FIGURE 11. Mutual coupling between output ports.

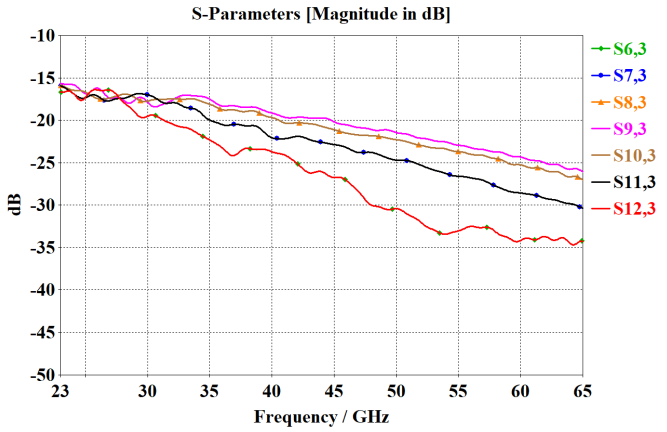

FIGURE 12. Transmission coefficients for port 3.

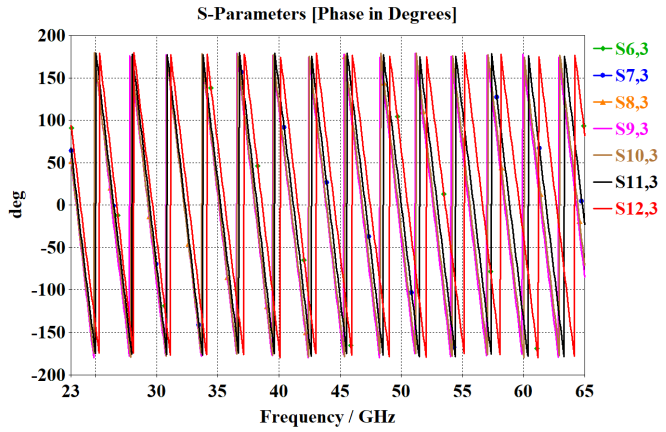

FIGURE 13. Phase of S-parameters of port 3.

beam ports. This outcome is expected, considering the closer proximity of transmission lines at the network ports relative to the beam ports. Nonetheless, the measured coupling levels remain below -15 dB, which is considered sufficient to ensure that the lens performance is not adversely affected.

3.4. Transmission Coefficients

The simulated transmission and phase coefficients between beam and array ports are shown in Figures 12 and 13. For the transmission coefficients, amplitude uniformity is a key requirement for stable beam steering. When port 3 is excited, the amplitudes remain below –15 dB across the bandwidth, with values between –16.94 dB and –17.79 dB at 28 GHz, confirming good energy distribution among the array ports within the 23–-65 GHz band. The phase response, obtained when the central port is excited, shows that the array ports are nearly in phase at 28 GHz, consistent with Rotman lens theory. Furthermore, the phase distribution is linear across the 23–-65 GHz range, leading to minimal fluctuations and reduced phase errors in the beamforming outputs.

3.5. Surface Current Distributions

Figures 14(a) to (e) presents the surface current distribution when each beam port (1–-5) of the proposed Rotman lens is excited separately. From these simulations, the majority of electric fields, as seen, propagate toward the output ports, and the evolving surface currents verify the design's high-performance operation. Additionally, there is essentially no coupling effect between the input ports, and some of the scattered waves are absorbed by the dummy ports. Consequently, the wireless subsystems enable beam-scanning operation with high effectiveness.

Table 2 presents a comparison with current Rotman lens designs according to size, bandwidth, isolation, and port number. It shows that Rotman lenses offer advantages such as wide bandwidth, low cost, and low mutual coupling. Moreover, the lens substrate uses only low-cost FR4, while maintaining acceptable insertion losses. As shown, most beamforming designs are limited in bandwidth, whereas the proposed Rotman lens achieves higher bandwidth up to 42 GHz than [3, 21, 39–45] along with an acceptable scanning range of $\pm 30°$. More importantly, the mutual coupling level in this work is significantly lower than those in [10, 29, 39–45] and comparable to [3, 5] which meets the requirements of 5G communication sys-

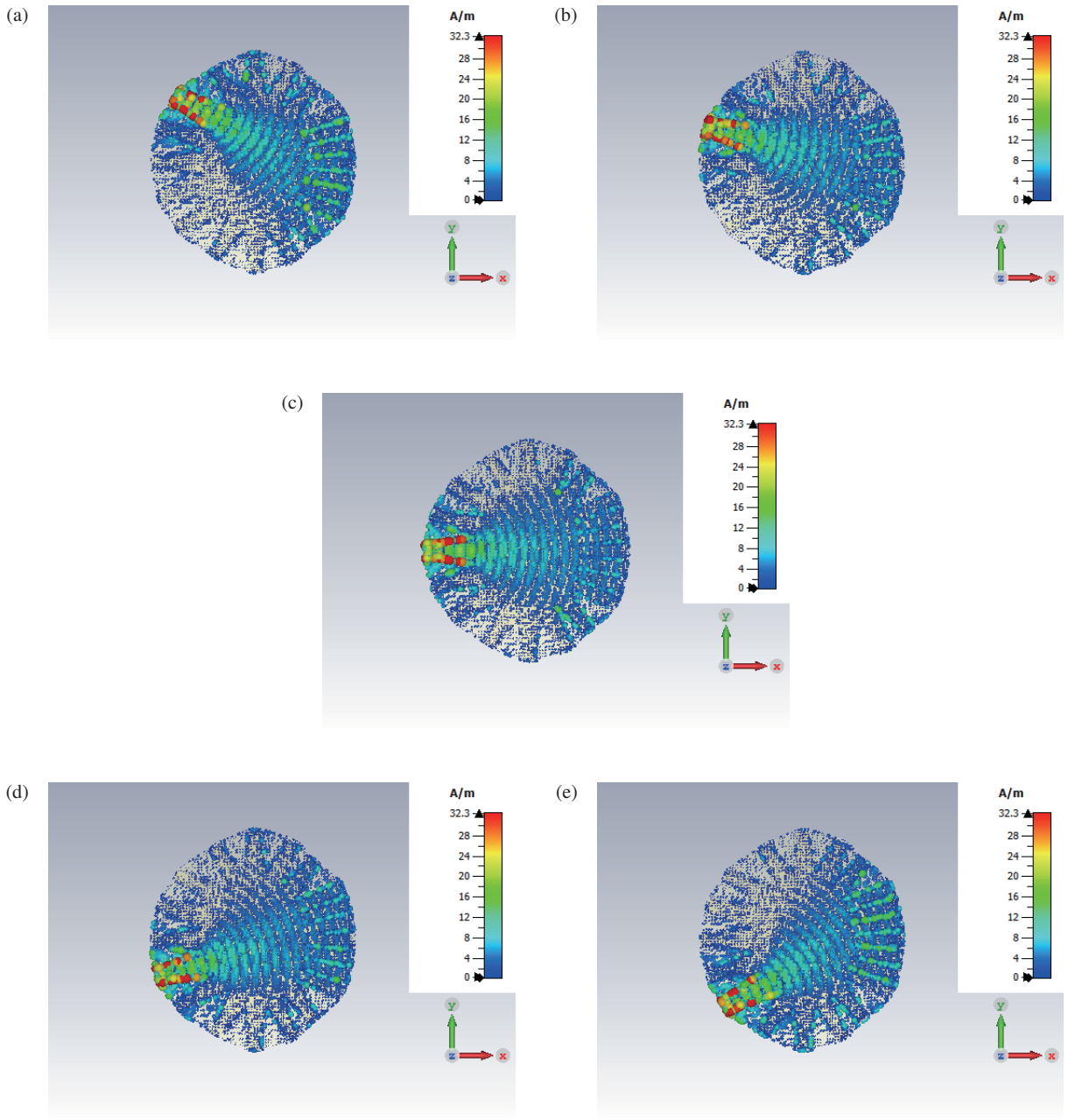

FIGURE 14. Surface currents of the proposed Rotman lens with single-port excitation: (a) port 1, (b) port 2, (c) port 3, (d) port 4, (e) port 5.

tems and demonstrates better performance than most other published works.

4. CONCLUSIONS

This work presents a Rotman lens comprising five beam ports and seven array ports, designed and implemented using low-cost PCB technology on an FR4 substrate. The proposed design realizes an ultra-wideband 5G MIMO beamforming module covering both the 28 GHz and 60 GHz mmWave bands, with an impedance bandwidth exceeding 100% (23–65 GHz), effectively spanning six standard 5G bands (n257, n258, n259, n260, n261, and n262). Performance evaluation using MATLAB and CST Microwave Studio demonstrated excellent results in terms of reflection and transmission coefficients, VSWR, and mutual coupling across the operating band, indicating good impedance matching, efficient energy transfer, and low losses. Comparative analysis with previously reported designs confirms the accuracy and reliability of the proposed structure. The proposed Rotman lens is suitable for a wide range of 5G and mmWave applications, including automotive radar, remote sensing, hybrid beamforming, and massive MIMO systems. Future work will focus on fabricating the proposed structure to experimentally validate its performance and compare measurement results with simulations. Furthermore, designing array antennas for multi-beam configurations will be considered to enhance the system's functionality and performance.

REFERENCES

[1] Joshi, M., K. Hu, C. A. Lynch, and M. M. Tentzeris, "Achieving quasi-planar coverage: A concave meniscus lens-enhanced Rotman lens based mmID for ultra-long range IoT applications," *IEEE Antennas and Wireless Propagation Letters*, Vol. 24, No. 3, 741–745, 2025.

[2] Mohamed, H. A. and M. Aboualalaa, "A low profile super UWB-MIMO antenna with d-shaped for satellite communications, 5G and beyond applications," *Scientific Reports*, Vol. 15, No. 1, 15660, 2025.

[3] Azari, A., A. Skrivervik, and H. Aliakbarian, "Design of a novel wide-angle Rotman lens beamformer for 5G mmWave applications," *Scientific Reports*, Vol. 14, No. 1, 1245, 2024.

[4] Najafabadi, A. M. A., F. Ballipinar, M. C. Tasdelen, A. Uzun, M. K. Yapici, A. Skrivervik, and I. Tekin, "Wide scan angle multibeam conformal antenna array with novel feeding for mm-wave 5G applications," *Microelectronic Engineering*, Vol. 294, 112261, 2024.

[5] Ali, M. S., H. Naveed, M. A. B. Abbasi, N. Shoaib, and V. F. Fusco, "Substrate-integrated coaxial line (SICL) rotman lens beamformer for 5G/B5G applications," *Electronics*, Vol. 12, No. 1, 69, 2023.

[6] Pant, M. and L. Malviya, "Design, developments, and applications of 5G antennas: A review," *International Journal of Microwave and Wireless Technologies*, Vol. 15, No. 1, 156–182, 2023.

[7] Ali, W. A. E., M. A. Abdelghany, and A. A. Ibrahim, "Wideband and high gain elliptically-inspired 4 × 4 MIMO antenna for millimeter wave applications," *Heliyon*, Vol. 10, No. 20, e38697, 2024.

[8] Najafabadi, A. M. A., F. A. Ghani, and I. Tekin, "Low-cost multibeam millimeter-wave array antennas for 5G mobile applications," *IEEE Transactions on Vehicular Technology*, Vol. 71, No. 12, 12 450–12 460, 2022.

[9] Azari, A., A. Skrivervik, H. Aliakbarian, and R. A. Sadeghzadeh, "A super wideband dual-polarized vivaldi antenna for 5G mmWave applications," *IEEE Access*, Vol. 11, 80 761–80 768, 2023.

[10] Saeed, M. A. and A. O. Nwajana, "A review of beamforming microstrip patch antenna array for future 5G/6G networks," *Frontiers in Mechanical Engineering*, Vol. 9, 1288171, 2024.

[11] Issa, K., H. Fathallah, M. A. Ashraf, H. Vettikalladi, and S. Alshebeili, "Broadband high-gain antenna for millimetre-wave 60-GHz band," *Electronics*, Vol. 8, No. 11, 1246, 2019.

[12] Saleem, I., M. A. B. Abbasi, N. Shoaib, S. Mukhopadhyay, H. Inaltekin, and S. M. Abbas, "Mitigation of radiation loss in mmwave rotman lens beamformers," in *2025 6th Australian Microwave Symposium (AMS)*, 1–2, Gold Coast, Australia, 2025.

[13] Rahimian, A., Y. Alfadhl, and A. Alomainy, "Analytical and numerical evaluations of flexible V-band Rotman lens beamforming network performance for conformal wireless subsystems," *Progress In Electromagnetics Research B*, Vol. 71, 77–89, 2016.

[14] Xiao, Z., L. Zhu, L. Bai, and X.-G. Xia, *Array Beamforming Enabled Wireless Communications*, CRC Press, 2023.

[15] Guo, Y. J. and R. W. Ziolkowski, *Advanced Antenna Array Engineering for 6G and Beyond Wireless Communications*, Wiley, 2021.

[16] Vashist, S., M. K. Soni, and P. K. Singhal, "A review on the development of Rotman lens antenna," *Chinese Journal of Engineering*, Vol. 2014, No. 1, 385385, 2014.

[17] Pezhman, M. M., A.-A. Heidari, and A. Ghafoorzadeh-Yazdi, "A novel single layer SIW 6 × 6 beamforming network for 5G applications," *AEU — International Journal of Electronics and Communications*, Vol. 155, 154380, 2022.

[18] Lian, J.-W., Y.-L. Ban, C. Xiao, and Z.-F. Yu, "Compact substrate-integrated 4 × 8 Butler matrix with sidelobe suppression for millimeter-wave multibeam application," *IEEE Antennas and Wireless Propagation Letters*, Vol. 17, No. 5, 928–932, 2018.

[19] Cao, Y., K.-S. Chin, W. Che, W. Yang, and E. S. Li, "A compact 38 GHz multibeam antenna array with multifolded butler matrix for 5G applications," *IEEE Antennas and Wireless Propagation Letters*, Vol. 16, 2996–2999, 2017.

[20] Hassanien, M. A., R. Hahnel, and D. Plettemeier, "Wideband rotman lens beamforming technique for 5G wireless applications," in *2019 2nd International Conference on Computer Applications & Information Security (ICCAIS)*, 1–5, Riyadh, Saudi Arabia, 2019.

[21] Kim, D.-W. and S.-S. Oh, "A volumetric waveguide-type rotman lens antenna for three-dimensional millimeter-wave beamforming," *Sensors*, Vol. 24, No. 9, 2884, 2024.

[22] Hong, H., H. Park, K. Lee, W. Lee, S. Jo, J. Yang, C. Park, H. Lee, and S. K. Hong, "Ka-band Rotman lens-based retrodirective beamforming system for wireless power transfer," *Journal of Electromagnetic Engineering and Science*, Vol. 21, No. 5, 391–398, 2021.

[23] Mujammami, E. H. and A. Sebak, "Analog beamforming system using rotman lens for 5G applications at 28 GHz," in *2019 IEEE International Symposium on Antennas and Propagation and USNC-URSI Radio Science Meeting*, 153–154, Atlanta, GA, USA, 2019.

[24] Eid, A., J. G. D. Hester, and M. M. Tentzeris, "Rotman lens-based wide angular coverage and high-gain semipassive architecture for ultralong range mm-wave RFIDs," *IEEE Antennas and Wireless Propagation Letters*, Vol. 19, No. 11, 1943–1947, 2020.

[25] Liang, Q., B. Sun, and G. Zhou, "Miniaturization of Rotman lens using array port extension," *IEEE Antennas and Wireless Propagation Letters*, Vol. 22, No. 3, 541–545, 2023.

[26] Sun, B.-h., Q.-y. Liang, and G.-n. Zhou, "Miniaturized Rotman lens with applications to wireless communication," *Frontiers of Information Technology & Electronic Engineering*, Vol. 21, No. 1, 144–158, 2020.

[27] Attaran, A., R. Rashidzadeh, and A. Kouki, "60 GHz low phase error Rotman lens combined with wideband microstrip antenna array using LTCC technology," *IEEE Transactions on Antennas and Propagation*, Vol. 64, No. 12, 5172–5180, 2016.

[28] Yu, Y., H. Luyen, and N. Behdad, "A wideband millimeter-wave Rotman lens multibeam array using substrate integrated coaxial line (SICL) technology," *IEEE Transactions on Antennas and Propagation*, Vol. 69, No. 11, 7532–7542, 2021.

[29] Lian, J.-W., Y.-L. Ban, and Y. J. Guo, "Wideband dual-layer huygens' metasurface for high-gain multibeam array antennas," *IEEE Transactions on Antennas and Propagation*, Vol. 69, No. 11, 7521–7531, 2021.

[30] Zhang, H. and A. Shamim, "Wideband and wide beam scanning dual-polarized phased array antenna-in-package design for 5G applications," *IEEE Open Journal of Antennas and Propagation*, Vol. 5, No. 1, 140–152, 2024.

[31] Ikram, M., K. Sultan, M. F. Lateef, and A. S. M. Alqadami, "A road towards 6G communication — A review of 5G antennas, arrays, and wearable devices," *Electronics*, Vol. 11, No. 1, 169, 2022.

[32] Rotman, W. and R. Turner, "Wide-angle microwave lens for line source applications," *IEEE Transactions on Antennas and Prop-*

agation, Vol. 11, No. 6, 623–632, 1963.

[33] Hansen, R. C., "Design trades for Rotman lenses," *IEEE Transactions on Antennas and Propagation*, Vol. 39, No. 4, 464–472, 1991.

[34] Smith, M. S., "Design considerations for Ruze and Rotman lenses," *Radio and Electronic Engineer*, Vol. 52, No. 4, 181–187, 1982.

[35] Simon, P., "Analysis and synthesis of Rotman lenses," in *22nd AIAA International Communications Satellite Systems Conference & Exhibit 2004 (ICSSC)*, 3196, Monterey, CA, USA, May 2004.

[36] Katagi, T., S. Mano, and S. Sato, "An improved design method of rotman lens antennas," *IEEE Transactions on Antennas and Propagation*, Vol. 32, No. 5, 524–527, 1984.

[37] Mujammami, E. H., I. Afifi, and A. B. Sebak, "Optimum wideband high gain analog beamforming network for 5G applications," *IEEE Access*, Vol. 7, 52 226–52 237, 2019.

[38] Tekkouk, K., M. Ettorre, and R. Sauleau, "SIW Rotman lens antenna with ridged delay lines and reduced footprint," *IEEE Transactions on Microwave Theory and Techniques*, Vol. 66, No. 6, 3136–3144, 2018.

[39] Prihatiningtyas, N. N., K. Anwar, and A. A. Pramudita, "Microstrip rotman lens for mobile base station backbone in disaster area networks," *International Journal on Advanced Science Engineering and Information Technology*, Vol. 12, No. 4, 1327, 2022.

[40] Ershadi, S. E., A. Keshtkar, A. Bayat, A. H. Abdelrahman, and H. Xin, "Rotman lens design and optimization for 5G applications," *International Journal of Microwave and Wireless Technologies*, Vol. 10, No. 9, 1048–1057, 2018.

[41] Liang, Q., B. Sun, G. Zhou, J. Zhao, and G. Zhang, "Design of compact Rotman lens using truncated ports with energy distribution slots," *IEEE Access*, Vol. 7, 120 766–120 773, 2019.

[42] Sethi, W. T., A. B. Ibrahim, K. Issa, and S. A. Alshebeili, "MmW Rotman lens-based sensing: An investigation study," *Sensors*, Vol. 21, No. 4, 1163, 2021.

[43] Lian, J.-W., H.-N. Wu, C. Geng, W. Hong, and D. Ding, "Compact millimeter-wave orthogonal SIW multibeam antenna based on shared-cavity rotman lens and shared-aperture array antenna," *IEEE Transactions on Antennas and Propagation*, Vol. 73, No. 8, 6169–6174, 2025.

[44] Chou, H.-T. and C.-Y. Chang, "Application of rotman lens beamformer for relatively flexible multibeam coverage from electrically large-phased arrays of antennas," *IEEE Transactions on Antennas and Propagation*, Vol. 67, No. 5, 3058–3066, 2019.

[45] Haro-Báez, R., J. Moreno, and D. S. Benítez, "On the design of a substrate integrated waveguide rotman lens for K-band applications," in *2020 IEEE Latin-American Conference on Communications (LATINCOM)*, 1–6, Santo Domingo, Dominican, 2020.